



Control of Mechanical Properties of Polyurethane Elastomers Synthesized with Aliphatic Diisocyanate Bearing a Symmetric Structure

Ken Kojio^{*,**,*†}, Shuhei Nozaki^{*}, Atsushi Takahara^{*,**,*†}, and Satoshi Yamasaki^{****}

^{*}Graduate School of Engineering, ^{**}Institute for Materials Chemistry and Engineering

^{***}WPI-FCNER, Kyushu University, 744 Motoooka, Nishi-ku, Fukuoka 819-0395, Japan

^{****}Mitsui Chemicals, Inc. 580-32, Nagaura, Sodegaura, Chiba 299-0265, Japan

(Received June 17, 2019, Revised July 22, 2019, Accepted July 23, 2019)

Abstract: Polyurethane elastomers (PUEs) were synthesized using *trans*-1,4-bis(isocyanatomethyl) cyclohexane (1,4-H₆XDI), poly(oxytetramethylene) glycol, 1,4-butanediol (BD), and 1,1,1-trimethylol propane (TMP). To control the molecular aggregation state and mechanical properties of these PUEs, hard segment contents of 20 and 30 wt% and BD/TMP ratios of 10/0 and 8/2 were chosen. Differential scanning calorimetry and small-angle X-ray scattering measurements revealed that the degree of microphase separation increased with an increase in both hard segment content and BD ratio. The Young's modulus and strain at break of the 1,4-H₆XDI-based PUE were 6–20 MPa and 5–15, respectively. Incorporation of 20% TMP as a cross-linking agent into BD increased the melting temperature of the hard segment chains, that is, heat resistance, and decreased the Young's modulus. This could be due to the low density of the physical cross-linking network and the dispersion of hard segment chains in the soft segment matrix in the PUE in the presence of 20% TMP.

Keywords: Polyurethane elastomers, mechanical properties, differential scanning calorimetry, small-angle X-ray scattering, Young's modulus

Introduction

Polyurethane elastomers (PUEs) exhibit versatile mechanical properties as one can see many applications like coating, adhesive, sealant, sealant, and so on.¹ The PUEs are basically composed of alternating hard and soft segments. Soft and hard segments are generally composed of polyether, polyester or polycarbonate-based glycol and diisocyanate and low molecular weight diol, respectively. The resulting polymeric PUE molecules form a microphase-separated structure depending on the thermodynamic immiscibility of the constituent segments. The hard segment chains occasionally are in the crystalline state with the formation of hydrogen-bonded. Since the molecular aggregation structure including the microdomain structure, the degree of microphase separation, and the hydrogen bonding state of hard segments are closely related to the mechanical property, investigation and control of the structure are quite important.

Since there are a very large number of starting materials for polymerization of PUE, the various properties can be

tuned by choice of materials, conditions, molar ratio and so on. For example, poly(oxytetramethylene) glycol (PTMG), 4,4'-diphenylmethane diisocyanate (MDI) and 1,4-butanediol (BD)-based PUE is well-known as to exhibit superior mechanical property.^{2,3} To complement lack property, for instance, flexibility, low Young's modulus, durability for light of PTMG-MDI-BD-based PUE, amorphous polyol, like poly(oxypropylene) glycol (PPG), cycloaliphatic/aliphatic diisocyanate^{4,6} and so on, should be employed. Recently, it was reported that *trans*-1,4-bis(isocyanatomethyl) cyclohexane (1,4-H₆XDI) exhibits superior property in terms of mechanical property and durability for light.^{7–9} However, the structure-property relationship of the 1,4-H₆XDI-based PUEs are not well understood and control of mechanical properties in the wide range has not been attained.

In this study, four types of 1,4-H₆XDI-based PUEs were synthesized with various hard segment content and BD/TMP ratio. The relationship between structure and properties of the 1,4-H₆XDI-based PUEs were studied by swelling test, infrared spectroscopy (IR), differential scanning calorimetry (DSC), wide-angle X-ray diffraction and small-angle X-ray scattering (WAXD and SAXS), dynamic viscoelastic property mea-

[†]Corresponding author E-mail: kojio@cstf.kyushu-u.ac.jp

surement and tensile testing.

Experimental section

1. Raw materials

Poly(oxytetramethylene) glycol (PTMG: number-average molecular weight (M_n)=1826, Asahi Kasei Chemicals Co., Ltd., Japan), *trans*-1,4-bis (isocyanatomethyl) cyclohexane (FORTIMOTM 1,4- H_6 XDI, Mitsui Chemicals Inc., Japan), 1,4-butanediol and 1,1,1-trimethylol propane (BD and TMP, Wako Chemicals Co., Ltd., Japan), were used as the polymer glycol, diisocyanate, chain extender, and cross-linking agent for polyurethane synthesis, respectively. BD was refluxed in the presence of calcium hydride to remove water and then purified by distillation. The amount of residual water was a few hundred ppm. FORTIMOTM 1,4- H_6 XDI was used without further purification. Impurity is choline derivative in ppm.

2. Preparation of 1,4- H_6 XDI-based PUEs

The PUEs prepared in this study were synthesized in bulk with PTMG, 1,4- H_6 XDI and BD and TMP. Figure 1 shows the synthetic scheme of a prepolymer method. The 1,4- H_6 XDI-based PUEs with two hard segment contents, 20 and 30 wt%, and two TMP contents, 0 and 20 wt%, were synthesized. The nomenclature denotes the type of diisocyanate, hard segment content, and BD/TMP ratio, for example, HX-30-8/2 denotes 1,4- H_6 XDI-based PUE with hard segment content of 30 wt%, and BD/TMP = 8/2.

PTMG was dried with dry nitrogen under reduced pressure using a separable flask prior polymerization. Prepolymers were synthesized from PTMG and excess 1,4- H_6 XDI with a mechanical agitator and a formulation ratio of $K=[NCO]_{HX}/[OH]_{PTMG}=3.0$ and 2.0 for HX-30 and HX-20, respectively, at 80°C for 3 hours under a nitrogen atmosphere, where $[NCO]_{HX}$ and $[OH]_{PTMG}$ are the number of moles of NCO groups and OH groups, respectively. 10 mg of dibutyltin dilaurate (DBTL, Wako Chemical Co., Ltd. Japan) was added as a catalyst in the prepolymer reaction. The extent of the polymerization reaction was pursued by an amine equivalent method and the end of the reaction was determined by confirming that reaction ratio of NCO groups exceeded 90%. After completing the prepolymer reaction, the prepolymer was degassed using a vacuum agitator. BD or a mixture of BD/TMP were added to the prepolymer obtained and agi-

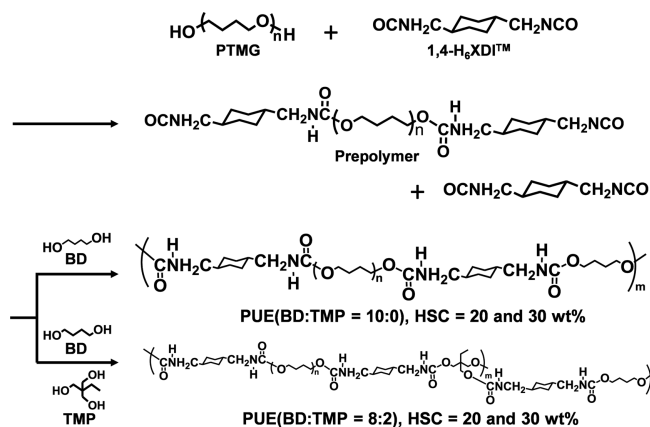


Figure 1. Synthetic scheme of PUEs by a prepolymer method.

tated in vacuo at a ratio of $[NCO]_{pre}/[OH]_{BD/TMP}=1.03$, where $[NCO]_{pre}$ and $[OH]_{BD/TMP}$ are the numbers of moles of NCO groups in the prepolymer and OH groups of BD and TMP, respectively. After mixing the viscous product for 90 s, it was poured into a mold constructed using a 1 mm thick spacer and two aluminum plates heated at 120°C. The PUEs were cured at 120°C for 24 h in air.

3. Swelling behaviors of PUEs

The swelling behavior of the 1,4- H_6 XDI PUEs was evaluated with toluene and *N,N*-dimethylacetamide (DMAc). Toluene and DMAc are non-polar and polar solvents, respectively. Prior to soak the sample to solvents, specimens were dried in vacuo for 24 hours. To swell the PUEs, specimens were soaked in each solvent at 60°C to attain the equilibrium swelled state. The gel fraction, G , was defined as $G=W_b/W$, where W_b and W are the dry weight after swelling and initial weight, respectively. Moreover, the degree of swelling, Q , of the PUEs was determined from weights of dry and swollen PUE samples. Q is defined as following equation, $Q=1+[(W_a-W_b)/d_s/(W_b/d_p)]$, where W_a , d_s and d_p are the weight of sample swollen to equilibrium state, the density of solvent, and density of the PUEs, respectively.

4. Hydrogen bonding state of urethane groups

The state of hydrogen bond of the hard and soft segments in the 1,4- H_6 XDI-based PUEs was evaluated by attenuated total reflection Fourier transform infrared spectroscopy (ATR-FT-IR). Spectra were obtained with an FTS-3000 EXCALIBUR (Bruker Japan Co., Ltd. Japan) equipped with a liquid N_2 cooled mercury cadmium telluride (MCT) detec-

tor using a ATR cell (MIRacle, PIKE Technologies, Inc. USA). All spectra were collected with 32 scans and at a resolution of 4 cm^{-1} .

5. Thermal behavior of PUEs

DSC measurement was performed to investigate glass transition temperature and melting point of the PUEs. The DSC curves were obtained using a DSC (Rigaku DSC 8230, Rigaku Denki Co. Ltd. Japan) in the temperature from -140 to 250°C under a nitrogen atmosphere. A heating rate was $10^\circ\text{C min}^{-1}$. At the start of measurement, as-prepared samples were simply cooled down to around -145°C .

6. Crystal structure of hard segment and microdomain structure

Small-angle X-ray scattering (SAXS) and wide-angle X-ray diffraction (WAXD) measurements were conducted for the PUEs at the BL03XU8,9 and BL05XU beamline in the SPring-8 facility in Japan. The photon flux was $\sim 10^{13}$ photons/s, and the size of beam at the sample was $150\text{ mm} \times 150\text{ mm}$. The wavelength of X-ray was 0.1 nm . For SAXS measurements, a CCD detector (ORCA-R2, Hamamatsu Photonics, K. K.) with a pixel size of 126 mm/pixel and a total size of 672×512 pixels was used to measure the scattered radiation. The detector was placed behind a vacuum path, and the camera length was ca. 2 m . For WAXD measurements, a flat panel detector was employed, and the camera length was 63 mm . Scattering patterns were collected for $200\sim 500\text{ ms}$. Data obtained were reduced from the 2D pattern to 1D profile with FIT2D (Ver. 12.077, Andy Hammersley). Both sets of data were expressed using the wave vector, q , where $q = 4\pi \sin \theta/\lambda$. Absolute scattering intensity was obtained by calibration with pure water.¹⁰

7. Temperature dependence of dynamic viscoelastic properties

The temperature dependence of dynamic viscoelastic properties were obtained with a DMS 6100 (Seiko Instruments, Co., Ltd., Japan) in the temperature range from -150 to 250°C with a heating rate of 2°C min^{-1} under a nitrogen atmosphere. The sample size was $25 \times 5 \times 2\text{ mm}^3$. Imposed strain and frequency were 0.2% and 10 Hz , respectively.

Table 1. Density, Gel Fraction, Degree of Swelling of 1,4-H₆XDI- and MDI-based PUEs

PU	Density (g/cm ³)	Degree of swelling		Gel fraction (%)	
		Toluene	DMAc*	Toluene	DMAc*
HX-30-10/0	1.06	3.24	18.2	99.3	23.5
HX-30-8/2	1.04	3.80	5.48	99.6	98.9
HX-20-10/0	1.04	4.20	soluble	99.2	soluble
HX-20-8/2	1.03	5.09	6.83	99.4	97.9

*N,N-Dimethyl acetamide

8. Uniaxial tensile test

Uniaxial tensile tests were carried out using an Instron type tensile tester (RTE-1210, Orientec, Co., LTD.) at 20°C . The dimension of samples were $5.0 \times 100.0 \times 1\text{ mm}^3$. An initial length and elongation rate were 30 mm and 10 mm min^{-1} ($33\% \text{ min}^{-1}$), respectively.

Results and Discussion

Appearances of all PUEs are milky opaque. This implies that crystallites are formed from the hard segment chains in the all PUEs. Table 1 shows density, gel fraction and degree of swelling of the PUEs. Gel fraction of the PUEs swollen by toluene was greater than 99%. This indicates that a well-developed network structure was formed in all PUEs. Also, gel fractions of HX-20-8/2 and HX-30-8/2 with chemical cross-linking points by DMAc was greater than 98%. This implies that a chemical cross-linking network was properly formed by incorporation of TMP. Furthermore, HX-20-10/0 was soluble in polar solvent, DMAc, in contrast to HX-30-10/0. The linear PUEs, which form only physical cross-links, dissolve in DMAc, because hydrogen bonds in physical cross-links dissociate when solvated by molecules of polar solvent.^{4,11-14} Thus, insolubility of HX-30-10/0 in DMAc suggests that HX-30-10/0 forms quite strong physical cross-links. The degree of swelling in toluene and DMAc for PUEs decreased with increasing hard segment content. This simply corresponds to the increase of cross-linking region, in other words, increase in cross-linking density. The degree of swelling of HX-30-8/2 and HX-20-8/2 by toluene exhibited greater value than for HX-30-10/0 and HX-20-10/0. For the MDI-based PUE, incorporation of TMP induces decrease in the degree of swelling due to additional incorporation of chemical network structure.¹² The reason why the 1,4-H₆XDI-based PUE showed opposite trend to MDI-based PUE is associated with the strong cohesive force of hard segment

chains, $-(1,4\text{-H}_6\text{XDI-BD})_n-$. That is, incorporation of TMP induced great decrease of ordering hard segment chains for the 1,4- H_6XDI -based PUE.

ATR-FT-IR measurements were carried out in order to evaluate hydrogen bonding state of the urethane carbonyl groups of hard segment chains and ether oxygen of soft segment chains in the PUEs. Figure 2 shows ATR-FT-IR spectra of (a) $3600\text{--}3200\text{ cm}^{-1}$ and (b) $1800\text{--}1600\text{ cm}^{-1}$ region for the four 1,4- H_6XDI -based PUEs prepared with various hard segment ratio and BD/TMP ratio. NH and carbonyl stretching bands ($\nu(\text{NH})$ and $\nu(\text{C=O})$) were clearly observed at around 3300 and 1700 cm^{-1} , respectively, for all PUEs. In all spectra, NCO stretching band was not observed at 2260 cm^{-1} , which indicates that the curing and cross-linking were properly occurred for all PUEs. The carbonyl stretching bands at 1660 cm^{-1} which is characteristic of allophanate groups were not also observed. The hydrogen bonding state in the hard segment chains can be ascertained from the absorbance of the $\nu(\text{NH})$ and $\nu(\text{C=O})$ bands.^{15,16} NH stretching bands forming hydrogen bonds with ether oxygen and carbonyl groups and free one are generally observed at around $3290\text{--}3310$, $3300\text{--}3350$ and 3450 cm^{-1} , respectively. On the contrary, the hydrogen bonded carbonyl stretching band ($\nu(\text{C=O}_{\text{H-bond}})$) and free one ($\nu(\text{C=O}_{\text{free}})$) are observed at around 1690 and 1725 cm^{-1} , respectively. Thus, bands observed at 3340 , 1693 and 1721 cm^{-1} in Figure 2 are likely to correspond to $\nu(\text{NH})$, $\nu(\text{C=O}_{\text{H-bond}})$ and $\nu(\text{C=O}_{\text{free}})$ bands, respectively. The ratios of $I_{\nu(\text{C=O}_{\text{H-bond}})}$ to $I_{\nu(\text{C=O}_{\text{free}})}$ ($I_{\nu(\text{C=O}_{\text{H-bond}})}/I_{\nu(\text{C=O}_{\text{free}})}$) for HX-30-10/0 and HX-20-10/0 were almost the same and much higher than for HX-30-8/2 and HX-20-8/2. Furthermore, the $\nu(\text{NH})$ band for HX-30-10/0 and HX-20-10/0 observed at 3340 cm^{-1} were sharper than

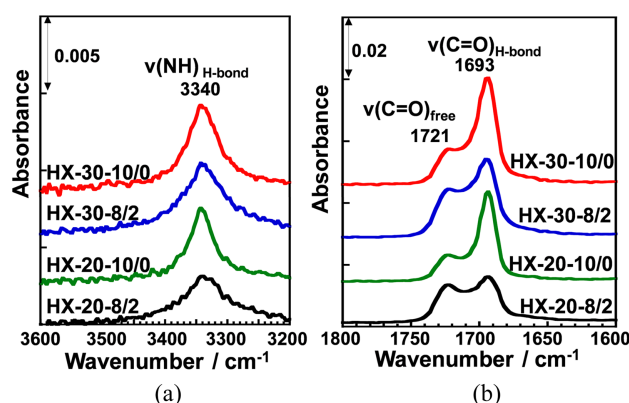


Figure 2. ATR-FT-IR spectra of the HX-30-10/0, HX-30-8/2, HX-20-10/0, and HX-20-8/2. (a) $3600\text{--}3200\text{ cm}^{-1}$ and (b) $1800\text{--}1600\text{ cm}^{-1}$.

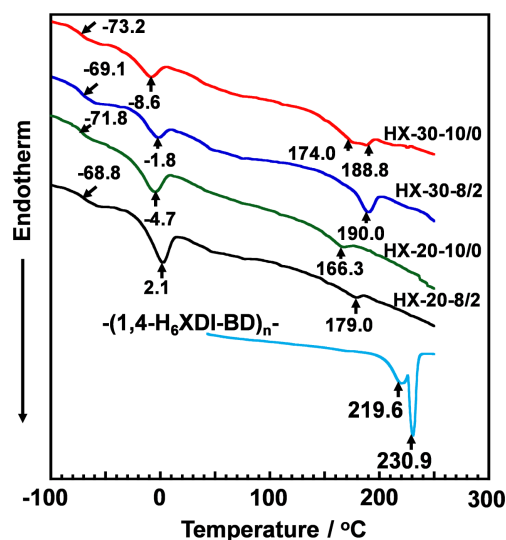


Figure 3. DSC thermograms of the HX-30-10/0, HX-30-8/2, HX-20-10/0, and HX-20-8/2.

for HX-30-8/2 and HX-20-8/2 and shifted to higher wave-number region. These results clearly indicate that the hard segment chains of HX-30-10/0 and HX-20-10/0 are well-organized and more strongly hydrogen bonded in comparison with HX-30-8/2 and HX-20-8/2.

Thermal behaviors of the PUEs were investigated by DSC. Figure 3 shows the DSC thermograms for the 1,4- H_6XDI -based PUEs prepared with various hard segment contents and BD/TMP ratio. Baseline shift and endothermic peaks were observed at around -70 , 0 , and 180°C for all PUEs. These can be assigned to the glass transition temperatures of the soft segment chains ($T_{g,s}$), melting of crystallized soft segment chains ($T_{m,s}$), and melting points of the crystallized hard segment domains ($T_{m,H}$ s). The $T_{g,s}$ and $T_{m,s}$ decreased with increases in hard segment content and decrease in TMP content. It is well known that the increasing T_g of the soft segment in PUE systems means an increasing miscibility of the two components on account of the molecular interaction between the soft and hard segments. Therefore, it is likely to consider that the soft segment phase with the richest state is in HX-30-10/0. On the contrary, for the hard segment chains, $T_{m,H}$ increased with increase in hard segment content and TMP content. Increase in TMP content seems to give appropriate length of hard segment chains to crystallize. Thus, it seems reasonable to consider that the degree of microphase separation became stronger with increase in hard segment content and decrease in BD content.

To investigate the crystal structure of the hard segment chains in the PUEs, WAXD measurements were carried out.

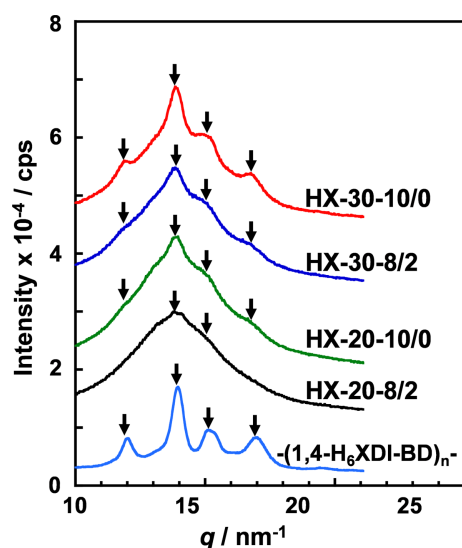


Figure 4. WAXD profiles of the HX-30-10/0, HX-30-8/2, HX-20-10/0, HX-20-8/2, and hard segment models.

Figure 4 shows WAXD profiles for the 1,4- H_6 XDI-based PUEs prepared with various hard segment contents and BD/TMP ratios. For comparison, the WAXD profiles of hard segment models for $-(1,4-H_6XDI-BD)_n-$ were also plotted. The crystalline peaks were clearly observed at $q = 12.0, 13.9, 15.2$ and 17.0 nm^{-1} for the $-(1,4-H_6XDI-BD)_n-$ model. These peak positions correspond well to those obtained for triclinic of P1 symmetry with $a = 0.736 \text{ nm}$, $b = 0.861 \text{ nm}$, $c = 1.784 \text{ nm}$, $\alpha = 140.9^\circ$, $\beta = 142.56^\circ$, $\gamma = 33.9^\circ$.⁷ For HX-30-10/0, HX-30-8/2 and HX-20-10/0, one can clearly see crystalline peaks at the same positions with the hard segment model, though some of them are difficult to recognize because of overlapping amorphous halo of soft segment. It is conceivable that

the hard segment chains are packed in the same crystal lattice even in the PUEs. The intensity of crystalline peak of HX-30-10/0 was much higher than that for HX-20-10/0. This is due to the formation of well-organized crystallized hard segment domains as well as increase in hard segment content.

The degree and size of microphase separated structure in the PUEs was investigated by SAXS measurement. Figure 5 shows 1D-SAXS profiles for the 1,4- H_6 XDI-based PUEs prepared with various hard segment contents and BD/TMP ratios. Broad scattering peaks observed in the q range from 0.1 – 0.8 nm^{-1} are associated with interdomain spacing of hard segment domains in a microphase-separated structure, which is comprised of the isolated hard segment domains and a surrounding soft segment matrix. Peak positions of HX-30 PUEs were lower than for HX20. To discuss in detail, interdomain spacings were determined by analyzing the three-dimensional correlation function. Moreover, diffuse phase boundary thickness of hard and soft segments was determined by analyzing the deviation from Porod's law. These quantities were obtained according to the calculation methods by Bonart *et al.*¹⁷ and Koberstein *et al.*¹⁸ Table 2 summarizes interdomain spacings calculated from peak positions using Bragg's law and determined by correlation function analysis. The relative degrees of overall microphase separation for the HD-30 were larger than for HD-20.

The boundary diffuseness $(\Delta\eta''/\Delta\eta''-1)$, sigmoidal and linear boundary thicknesses (σ and E) of HX-30 were slightly larger than for HX-20. Moreover, the magnitudes of HX-30-8/2 were smaller than for HX-30-10/0 and HX-20 did not show clear trend. The PUEs containing large amount of

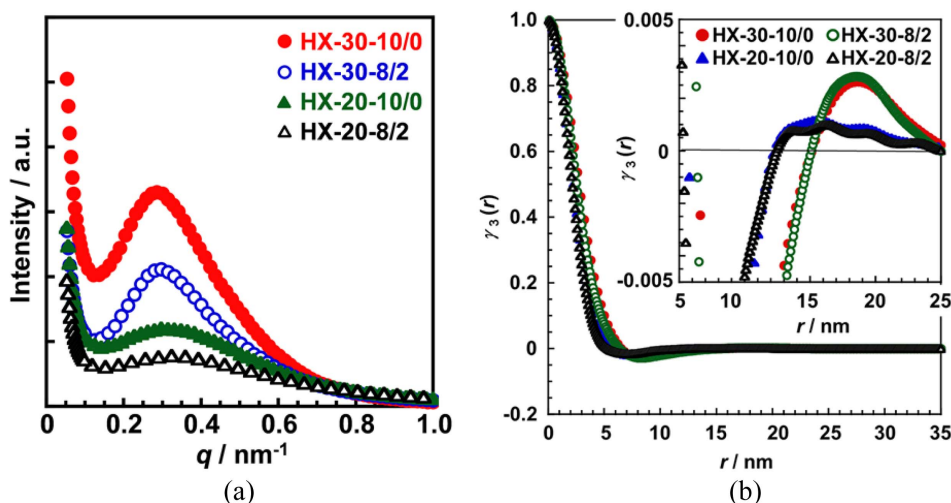


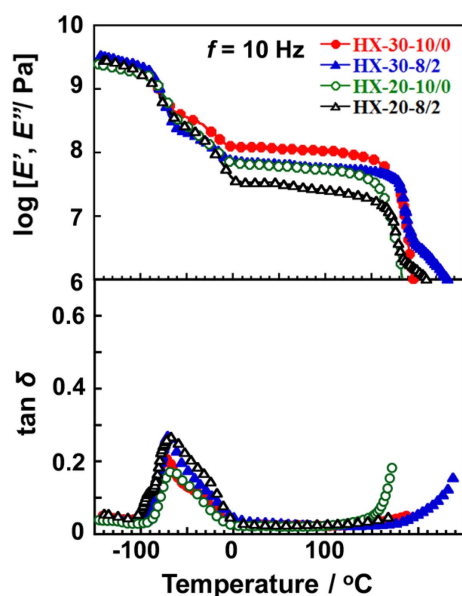
Figure 5. (a) SAXS profiles and (b) three-dimensional experimental correlation functions of the HX-30-10/0, HX-30-8/2, HX-20-10/0, and HX-20-8/2.

Table 2. Degree of Overall Microphase Separation, Diffuse-microphase Boundary Thickness Parameters for 1,4-H₆XDI-based PUEs

	Degree of overall microphase separation	Boundary diffuseness	Diffuse-microphase boundary thickness/nm		d-spacing from Bragg's law/nm	d-spacing from 3D correlation function/nm
	$\Delta\eta^2/\Delta\eta_c^2$	$\Delta\eta^2/\Delta\eta_c^2-1$	Sigmoidal, σ	Linear, E		
HX-30-10/0	0.39	1.77	0.84	2.09	17.4	18.1
HX-30-8/2	0.23	0.66	0.62	1.56	16.3	17.9
HX-20-10/0	0.29	0.18	0.35	0.88	16.4	16.7
MD-20-8/2	0.18	0.21	0.36	0.89	14.3	14.7

hard segments form larger hard segment domains, and they show larger boundary diffuseness. Incorporation of TMP reduced the size of hard segment domains, resulting decrease in boundary diffuseness and thickness. The boundary diffuseness and thickness are affected by the length and its distribution of hard segments, an aggregation force, and formation ability of hard segment domains.

Figure 6 shows dependence of the dynamic storage modulus (E'), loss modulus (E''), and loss tangent ($\tan\delta$) of the 1,4-H₆XDI-based PUEs on temperature with various hard segment contents and BD/TMP ratios. The E' and $\tan\delta$ values of all 1,4-H₆XDI-based PUEs steeply decreased and increased at around -70°C during the heating process. These changes are associated with the glass transition of the soft segments. Above the glass transition of the soft segment chain, a shoulder in E' curve at around -40°C was observed. This can be assigned to recrystallization of the soft segment. On the contrary, two dispersions were clearly observed from

**Figure 6.** Temperature dependence of dynamic viscoelastic properties of the HX-30-10/0, HX-30-8/2, HX-20-10/0, and HX-20-8/2.

-100 to 0°C in the $\tan\delta$ curve. They correspond to the glass-rubber transition and recrystallization of the soft segment chains during the heating process as discussed above. The rubbery plateau region was observed from 0 to 150°C for all the PUEs. The order of the E' value at the rubbery plateau region was as follow: HX-30-10/0 > HX-30-8/2 > HX-20-10/0 > HX-20-8/2. Further discussion on the E' values at rubbery plateau region will be given with Young's modulus by stress-strain curve. The terminal temperatures of HX-30 were higher than for HX-20, and also the temperatures of HX-30-8/2 and HX-20-8/2 were higher than for HX-30-10/0 and HX-20-10/0. In other words, increase in hard segment content and incorporation of TMP increased terminal temperature. These results are quite consistent with the fact that increase in hard segment content and TMP content increased $T_{m\rightarrow H}$ as observed by DSC.

Figure 7 shows stress-strain curves of the 1,4-H₆XDI-based PUEs with various hard segment contents and BD/TMP ratios. The Young's moduli estimated from an initial slope of stress-strain curves, tensile strength and strain at break value for the PUEs are summarized in Table 3. Young's modulus and tensile strength increased with an increase in hard segment content. Young's modulus decreased with increasing TMP content. HX-30-8/2 and HX-20-8/2 exhibited much larger slope in the larger strain region in comparison with HX-30-10/0 and HX-20-10/0. This is due to decreasing size

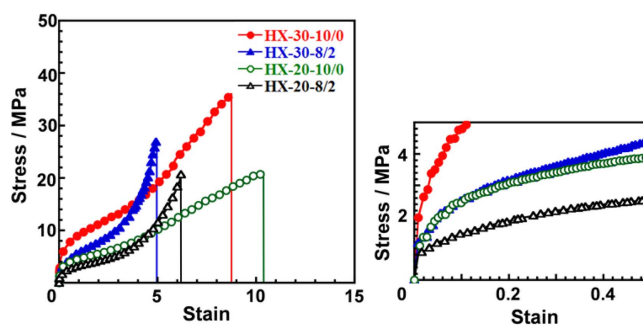
**Figure 7.** Stress-strain curves of the HX-30-10/0, HX-30-8/2, HX-20-10/0, and HX-20-8/2.

Table 3. Mechanical Properties of the 1,4-H₆XDI- and MDI-based PUEs Obtained from Stress-Strain Curves

Sample	Young's modulus/MPa	Strain at break	Tensile strength/MPa
HX-30-10/0	19.1	8.8	36.6
HX-30-8/2	11.4	5.0	27.4
HX-20-10/0	8.0	14.5	18.5
MD-20-8/2	6.1	6.1	20.7

of well-developed hard segment domains induced and chemical cross-linking points existing in the soft segment matrix by incorporation of TMP. For HX-30-10/0 and HX-20-10/0, the slope in the larger strain region were quite small and strain at break were around 10. HX-30-10/0 and HX-20-10/0 possess well-developed cylindrical hard segment domains.⁷ Thus, it is likely that obvious breaks of anisotropic cylindrical hard segment domains might have occurred for HX-based PUEs.

Conclusions

Four 1,4-H₆XDI-based PUEs with two different hard segment contents (20 and 30 wt%) and BD/TMP ratios (10/0 and 8/2) (HX-30-10/0, HX-30-8/2, HX-20-10/0, and HX-20-8/2) were synthesized with PTMG as a soft segment. The hard segment chains in the 1,4-H₆XDI-based PUEs crystallized easily forming strong intermolecular hydrogen bonds due to the symmetry of 1,4-H₆XDI molecule. It was revealed that the degree of microphase-separation increased with an increase in hard segment content and BD ratio. Young's modulus and strain at break were controlled in the ranges between 6 to 20 MPa and 5 to 15, respectively. These values are comparable with those for commercial 4,4'-diphenylmethane diisocyanate (MDI)-based PUEs, which are the one of the most popular PUEs in terms of mechanical properties. Furthermore, 1,4-H₆XDI's lack of aromatic moieties is expected to greatly enhance color stability of resulting PUEs.^{7,19} All the above features suggest 1,4-H₆XDI could replace MDI in a range of applications.

Acknowledgment

This work was supported by the Impulsing Paradigm Change through Disruptive Technology (ImPACT) Program and the Photon and Quantum Basic Research Coordinated Development Program from the Ministry of Education, Cul-

ture, Sports, Science and Technology, Japan. The part of wide-angle X-ray diffraction (WAXD) measurements were done at BL05XU in SPring-8 with the approval of RIKEN. WAXD measurements were also conducted at BL03XU and BL40XU in the SPring-8 facility with the approval of the Japan Synchrotron Radiation Research Institute (JASRI; Proposal No. 2012B1506, 2013B1186, 2014B1198, 2014B7266, 2015A1514, 2015A7216, 2015B7267, 2016A7217, 2016B7266, 2017A7215, 2017B7267). We gratefully acknowledge Dr. Hiroyasu Masunaga and Dr. Taizo Kabe (Japan Synchrotron Radiation Research Institute (JASRI)), Dr. Hiroki Ogawa (Kyoto University) for their assistance on the WAXD measurements.

References

1. Z. S. Petrovic and J. Ferguson, "Polyurethane elastomers", *Prog. Polym. Sci.*, **16**, 695 (1991).
2. Z. S. Petrovic and J. Budinski-Simendic, "Study of the effect of soft segment length and concentration on properties of polyetherurethanes. I. The effect on physical and morphological properties", *Rubber Chem. Technol.*, **58**, 685 (1985).
3. Z. S. Petrovic and J. Budinski-Simendic, "Study of the effect of soft segment length and concentration on properties of polyetherurethanes. I. The effect on physical and morphological properties", *Rubber Chem. Technol.*, **58**, 701 (1985).
4. K. Kojio, T. Fukumaru, and M. Furukawa, "Highly softened polyurethane elastomer synthesized with novel 1,2-bis(isocyanate)ethoxyethane", *Macromolecules*, **37**, 3287 (2004).
5. K. Kojio, S. Nakashima, and M. Furukawa, "Microphase-separated structure and mechanical properties of norbornane diisocyanate-based polyurethanes", *Polymer*, **48**, 997 (2007).
6. Y. Higaki, K. Suzuki, Y. Oniki, K. White, N. Ohta, and A. Takahara, "Molecular aggregation structure evolution during stretching of environmentally benign lysine-based segmented poly(urethane-urea)s", *Polymer*, **78**, 173 (2015).
7. S. Nozaki, S. Masuda, K. Kamitani, K. Kojio, A. Takahara, G. Kuwamura, D. Hasegawa, K. Moorthi, K. Mita, and S. Yamasaki, "Superior Properties of Polyurethane Elastomers Synthesized with Aliphatic Diisocyanate Bearing a Symmetric Structure", *Macromolecules*, **50**, 1008 (2017).
8. R. Rahmawati, S. Nozaki, K. Kojio, A. Takahara, N. Shinohara, and S. Yamasaki, "Microphase-separated structure and mechanical properties of cycloaliphatic diisocyanate-based thiourethane elastomers", *Polym. J.*, **51**, 265 (2019).
9. K. Kojio, R. Rahmawati, N. Shinohara, and S. Yamasaki, "Molecular Aggregation Structure and Mechanical Properties of Low-Hard Segment Content Polyurethane and Polythio-

- urethane Elastomers Based on Cycloaliphatic Diisocyanate with a Symmetric Structure”, *J. Adhes. Soc. Jpn.*, **55**, 181 (2019).
10. D. Orthaber, A. Bergmann, and O. Glatter, “SAXS experiments on absolute scale with Kratky systems using water as a secondary standard”, *J. Appl. Crystallogr.*, **33**, 218 (2000).
 11. M. Furukawa, Y. Hamada, and K. Kojio, “Aggregation structure and mechanical properties of functionally graded polyurethane elastomers”, *J. Polym. Sci., Part B: Polym. Phys.*, **41**, 2355 (2003).
 12. K. Kojio, S. Nakamura, and M. Furukawa, “Effect of side methyl groups of polymer glycol on elongation-induced crystallization behavior of polyurethane elastomers”, *Polymer*, **45**, 8147 (2004).
 13. K. Kojio, Y. Nonaka, T. Masubuchi, and M. Furukawa, “Effect of the composition ratio of copolymerized poly(carbonate) glycol on the microphase-separated structures and mechanical properties of polyurethane elastomers”, *J. Polym. Sci., Part B: Polym. Phys.*, **42**, 4448 (2004).
 14. K. Kojio, M. Furukawa, S. Motokucho, M. Shimada, and M. Sakai, “Structure–Mechanical Property Relationships for Poly(carbonate urethane) Elastomers with Novel Soft Segments”, *Macromolecules*, **42**, 8322 (2009).
 15. C. M. Brunette, S. L. Hsu, and W. J. Macknight, “Hydrogen-bonding properties of hard-segment model compounds in polyurethane block copolymers”, *Macromolecules*, **15**, 71 (1982).
 16. H. S. Lee, Y. K. Wang, and S. L. Hsu, “Spectroscopic analysis of phase-separation behavior of model polyurethanes”, *Macromolecules*, **20**, 2089 (1987).
 17. R. Bonart and E. H. Muller, “Phase separation in urethane elastomers as judged by low-angle x-ray-scattering. 2. Experimental results”, *J. Macromol. Sci. Phys.*, **B 10**, 345 (1974).
 18. J. T. Koberstein and R. S. Stein, “Small-angle x-ray-scattering studies of microdomain structure in segmented polyurethane elastomers”, *J. Polym. Sci., Part B: Polym. Phys.*, **21**, 1439 (1983).
 19. G. Kuwamura, T. Nakagawa, D. Hasegawa, and S. Yamasaki, “Bis(isocyanatomethyl)cyclohexane for making polyurethane resin useful for various applications”, WO2009051114A1 (2009).